Chapter 3

Imaging through dynamic scattering media

3.1 Introduction

When light passes through inhomogeneous-refractive-index media such as ground glass, living biological tissues, fog, turbid water, and atmospheric turbulence, scrambling of light's wavefront occurs, resulting in speckles, presenting significant challenges for optical imaging. In such cases, conventional and white-light imaging techniques fail to provide helpful information from the speckle. Over the years, numerous methods have been proposed to address the challenge of imaging through random scattering media [287–300]. Speckle patterns possess inherent statistical properties that can be utilized to recover the desired information. Statistical correlation methods exploit these features, providing a robust framework for imaging in the presence of randomness. In 1956, Hanbury Brown and Twiss (HBT) conducted a groundbreaking experiment using light intensity correlations to measure stars' angular diameter [173,301]. Later on, this HBT approach has motivated extensive studies of higher-order correlations in optics and high energy physics, nuclear physics, condensed matter, atomic physics [175,227,302–304], and so on. The HBT effect has been widely used in speckle contrast imaging [180], ghost imaging [182], optical coherence tomography [305], interferometry [306], physical optics [307,308], photon correlation imaging [185], etc. The simplicity and stability of the HBT technique make it an attractive method for characterizing correlation parameters and developing imaging techniques to see through randomness. Recent advancements have used intensity correlations to uncover the angular memory effect of speckles, which enables scattering media to function as lenses, making it possible to visualize objects obscured by random scatterers [153]. However, the intensity correlations provide only the amplitude of the object, and therefore, the phase information of the object is lost [185,309]. However, this missing phase information is crucial because it contains information about the internal structure and scattering events that have taken place inside

the object. Therefore, to reconstruct the complete object information, phase recovery becomes essential.

Intensive research efforts have been made to overcome phase loss issues in the intensity correlations by phase iterations [164,167]. These approaches leverage the angular memory effect and employ iterative phase retrieval algorithms to extract the phase information of the object. Despite their potential, challenges such as selecting appropriate support constraints and ensuring algorithm convergence have limited their practical applications [84–86,310,311]. More recently, novel imaging modalities based on intensity correlations have emerged for imaging through highly scattering media [312], including high-resolution fluorescence imaging using speckle illumination combined with speckle correlation [313,314].

Holographic techniques developed by Goodman et al. [315], Kogelnik and Pennington [316] offer a promising alternative for imaging through scattering media. Unlike iterative methods, holography does not suffer from convergence issues. Advances in this field have led to the development of non-iterative correlation holography techniques, which combine holography with intensity correlations to reconstruct complex object information [159,162,176,177,186,187,225,317–319]. These methods utilize various experimental designs incorporating the HBT approach to image objects obscured by static random diffusers.

However, the requirement that the scattering medium be static during the imaging process puts a constraint on the application of these techniques in a dynamic scattering scenario [320]. To overcome this, techniques such as speckle correlography, which adapts the shower curtain effect to the spatial-frequency domain, have been proposed [321].

Additionally, correlation imaging methods in different frequency regimes and wave control techniques for scattering media have emerged as viable solutions [322–326].

Dynamic scattering environments, such as those caused by dense fog or heavy rain, lead to rapid temporal decorrelation of optical information, posing further challenges for imaging [327,328]. Under such conditions, detecting instantaneous intensities and employing digital correlation methods can provide a suitable approach to developing state-of-the-art imaging techniques through dynamic scattering media. Postnov et al. demonstrated a dynamic light scattering imaging technique using a high-speed camera to record temporally fluctuating speckle patterns and reconstruct object information through temporal intensity autocorrelation functions [329]. Holographic approaches have also been adapted for imaging with temporally fluctuating fields, enabling their application in foggy or dynamic environments [330–334].

Building upon these advancements, we have developed alternative techniques specifically designed for imaging under dynamic scattering conditions, such as through a dynamic diffuser or fog, and two experimental techniques are presented in this chapter. In these techniques, objects passing through dynamic scattering media generate rapidly decorrelating intensity patterns, and we measure capturing a set of instantaneous random intensity patterns with a high-speed camera. Subsequent intensity correlations of these dynamic intensity patterns recover the object information encoded into the complex spatial coherence of the light at the detector plane and then subsequently use it for imaging. Our techniques are free from iterations and convergence issues of the phase retrieval algorithm and rely on the superposition of the coherence waves. A detailed theoretical basis and experimental results of the technique are presented below.

3.2 Theoretical basis of HBT correlation

Here, we discuss using intensity correlations in developing imaging techniques through dynamic scattering media. The basic principle of the technique is explained below.

Let us consider a stochastic, wide-sense stationary, paraxial beam propagation from the source to the observation plane as sketched in Fig. 3.1. The source is considered at the *z*=0 plane. The position vectors $\boldsymbol{\rho}$ and $\boldsymbol{r}$ denote a spatial position at the transverse source and observation planes, respectively.

A single realization of the complex amplitude distribution immediately behind the dynamic scattering medium is described as follows

$$U(\boldsymbol{\rho},t) = \left|U(\boldsymbol{\rho})\right| \exp\left[i\left(\psi(\boldsymbol{\rho}) + \phi(\boldsymbol{\rho},t)\right)\right] \tag{3.1}$$

where, $\left|U(\boldsymbol{\rho})\right|$ and $\psi(\boldsymbol{\rho})$ are amplitude and phase of the non-stochastic object and $\phi(\boldsymbol{\rho},t)$ is a random phase introduced by dynamic scattering media at a particular instant of time *t*. The corresponding realization of the complex field at the observation plane is represented by

$$U(\boldsymbol{r},t) = \int U(\boldsymbol{\rho},t) G\left(\boldsymbol{r}-\boldsymbol{\rho}\right) d\boldsymbol{\rho}, \tag{3.2}$$

where, $G\left(\boldsymbol{r}-\boldsymbol{\rho}\right)$ is the propagation kernel. Therefore, the intensity of a single realization of the field at the observation plane is represented as

$$I\left(\boldsymbol{r},t\right) = \left|U(\boldsymbol{r},t)\right|^2, \tag{3.3}$$

Where $U(\boldsymbol{r},t)$ is a field realization at a point $\boldsymbol{r}$ and at a time *t*. For simplicity, we can suppress the dependency on time '*t*' in our notations. The intensity is a random quantity, and its fluctuation over its mean value is represented as

$$\Delta I(\boldsymbol{r}) = I(\boldsymbol{r}) - \langle I(\boldsymbol{r}) \rangle, \tag{3.4}$$

where angular bracket $\langle \ \rangle$ represents the ensemble average and $\langle I(\boldsymbol{r}) \rangle$ represent the mean intensity. The statistical properties of such beam can be characterized by correlation of the intensity fluctuations, which is represented as

$$C(\boldsymbol{r_1}, \boldsymbol{r_2}) = \langle \Delta I(\boldsymbol{r_1}) \Delta I(\boldsymbol{r_2}) \rangle = \langle I(\boldsymbol{r_1}) I(\boldsymbol{r_2}) \rangle - \langle I(\boldsymbol{r_1}) \rangle \langle I(\boldsymbol{r_2}) \rangle, \tag{3.5}$$

Considering that the random fluctuations of the source follow a Gaussian process, the second-order correlation can be expressed in terms of the first-order correlations [67] as

$$C(\boldsymbol{r_1}, \boldsymbol{r_2}) = |W(\boldsymbol{r_1}, \boldsymbol{r_2})|^2 . \tag{3.6}$$

where, $W(\boldsymbol{r_1}, \boldsymbol{r_2}) = \langle U^*(\boldsymbol{r_1}) U(\boldsymbol{r_2}) \rangle$ represents the complex coherence function, which measures the beam's first-order statistical (coherence) properties. The complex coherence function is generally a complex quantity, with amplitude and phase distributions. Thus, the correlation of the intensity fluctuations provides the squared modulus of the complex coherence function, and phase is lost. Recently, few methods have been developed to measure complex coherence functions using generalized HBT interferometry, with interests in imaging through a static scattering medium [335–337].

In our technique, we recover the phase from the correlation of the intensity fluctuations. To apply our technique for imaging through a dynamic scattering medium, we introduce the concept of superposition of the coherence waves coming from the object and a reference field. Let us now consider that a complex field realization at the observation plane is represented as a coherent sum of two independent fields as

$$U_s(\boldsymbol{r}) = U(\boldsymbol{r}) + U_R(\boldsymbol{r}), \tag{3.7}$$

where, $U_R(\boldsymbol{r})$ is a reference field, and the intensity of a single realization at the observation plane becomes

$$I_s(\boldsymbol{r},t) = |U_s(\boldsymbol{r},t)|^2, \tag{3.8}$$

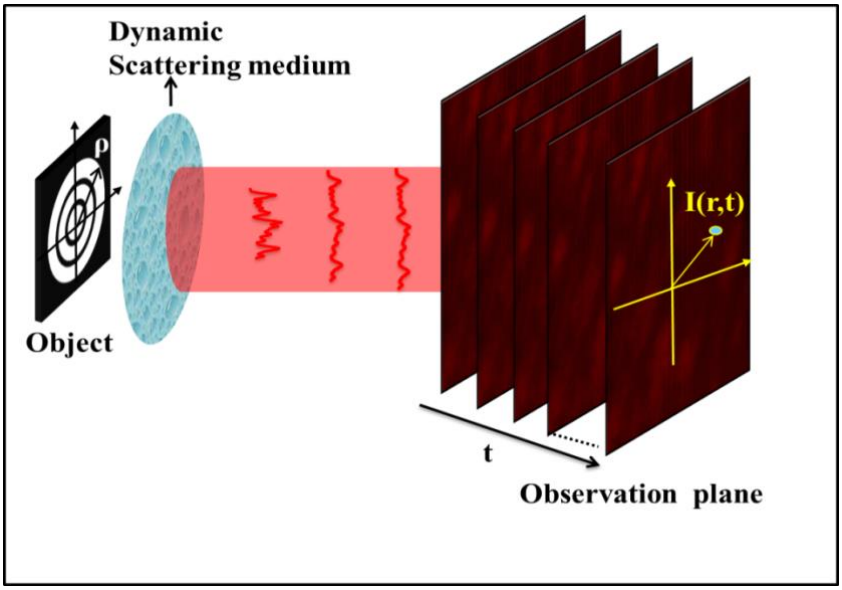

Fig. 3.1 Propagation from source to observation plane through a dynamic scattering medium.

Thus, the correlation of intensity fluctuations, as depicted in Eq. (3.6) becomes

$$C_s(\boldsymbol{r_1},\boldsymbol{r_2}) = |W_s(\boldsymbol{r_1},\boldsymbol{r_2})|^2 = |W(\boldsymbol{r_1},\boldsymbol{r_2})|^2 + |W_R(\boldsymbol{r_1},\boldsymbol{r_2})|^2 + W(\boldsymbol{r_1},\boldsymbol{r_2})W_R^*(\boldsymbol{r_1},\boldsymbol{r_2}) + W^*(\boldsymbol{r_1},\boldsymbol{r_2})W_R(\boldsymbol{r_1},\boldsymbol{r_2}) \tag{3.9}$$

where, $W_R(\boldsymbol{r_1},\boldsymbol{r_2}) = \langle U_R^*(\boldsymbol{r_1})U_R(\boldsymbol{r_2})\rangle$ represents the complex coherence function for the reference field. Eq. (3.9) is derived based on $\langle U^*(\boldsymbol{r_1})U_R(\boldsymbol{r_2})\rangle \approx 0$, due to statistically independent fields in Eq. (3.7).

Note that the intensity correlation hologram in Eq. (3.9) looks similar to the conventional holographic expression. Moreover, an intensity correlation hologram can be recorded in a

lensless Fourier configuration, as shown in Fig. 3.2. Eq. (3.9) states that the desired complex coherence function is now preserved and recoverable from the intensity correlation. The reference coherence function $W_R(\boldsymbol{r_1},\boldsymbol{r_2})$ covers the support of the object's coherence function $W(\boldsymbol{r_1},\boldsymbol{r_2})$ to record the fringes in the intensity correlation. Fourier fringe analysis of Eq. (3.9) helps to recover the object's complex coherence function, $W(\boldsymbol{r_1},\boldsymbol{r_2})$. In the Fourier fringe analysis, a Fourier transform of Eq. (3.9) consists of four terms as follows

$$FT\left\{\left|W_s(\boldsymbol{r_1},\boldsymbol{r_2})\right|^2\right\} = FT\left\{W(\boldsymbol{r_1},\boldsymbol{r_2})\right\}\otimes FT\left\{W^*(\boldsymbol{r_1},\boldsymbol{r_2})\right\} + FT\left\{W_R(\boldsymbol{r_1},\boldsymbol{r_2})\right\}\otimes FT\left\{W_R^*(\boldsymbol{r_1},\boldsymbol{r_2})\right\}$$
$$+FT\left\{W(\boldsymbol{r_1},\boldsymbol{r_2})\right\}\otimes FT\left\{W_R^*(\boldsymbol{r_1},\boldsymbol{r_2})\right\} + FT\left\{W^*(\boldsymbol{r_1},\boldsymbol{r_2})\right\}\otimes FT\left\{W_R(\boldsymbol{r_1},\boldsymbol{r_2})\right\}. \quad (3.10)$$

where, $\otimes$ and FT{.} represent two-dimensional (2D) convolution and Fourier transform, respectively. The first two terms on the right-hand side of Eq. (3.10) represent the central DC, which is digitally suppressed. The third and fourth terms containing the object information can be separated from central DC using a reference coherence function with a uniform amplitude profile and a linear phase. Finally, this recovered complex coherence function is used to image the object through the dynamic scattering medium by establishing a Fourier transform relation.

This chapter explores dynamic scattering scenarios and designs new experimental techniques for imaging through dynamic scattering media. Two different dynamic media are considered here for experimental validation of our approach, providing a comprehensive framework for imaging through dynamic scattering media, such as dynamic diffuser, fog, etc. These two experimental techniques are discussed below.

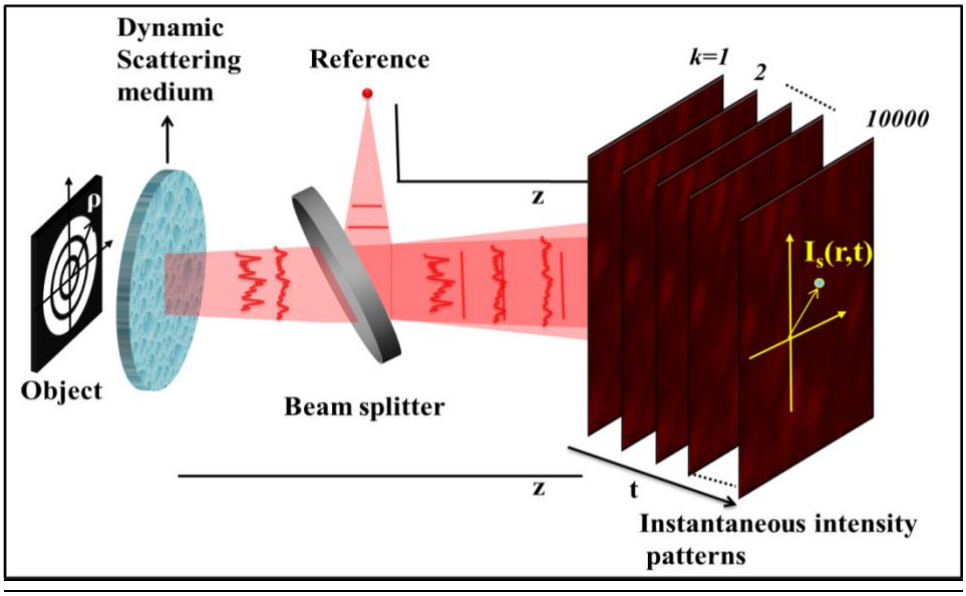

Fig. 3.2 Instantaneous intensity patterns recorded in a lensless configuration through a dynamic scattering medium.

3.3 Imaging through a dynamic scattering wall

This technique uses intensity correlations combined with a holographic approach for imaging through a dynamic scattering wall. For this purpose, we have designed a holographic setup to effectively interfere with the coherence waves coming from the object and a reference. Subsequently, superposed dynamically fluctuating intensity patterns are recorded with a high-speed detector. Intensity correlations of these dynamically fluctuating intensity patterns are used to retrieve the object information. Experimental setup and results are discussed in the coming sections.

3.3.1 Experiment

To illustrate the feasibility of our proposed technique, we present a proof of principle experiment, as shown in Fig. 3.3. In our experimental system, we used a He-Ne laser beam at 632nm to illuminate a dynamic scattering medium. A rotating ground glass (RGG) realizes this dynamic scattering medium. The beam from the RGG plate is regarded as an incoherent source as the beam spot size on the RGG plate is much larger

than the characteristic inhomogeneity scale of the RGG plate, and a set of independent random phases is introduced to mimic an incoherent source. An experimental geometry is used in such a way that objects and reference fields propagate through different dynamic diffusers, i.e., different positions of the RGG, as shown in Fig. 3.3. A series of rapidly decorrelating intensity patterns emerge due to RGG, and a high-speed camera is used to capture the dynamically fluctuating intensity patterns. To display the different objects with spatial features at the RGG, we used a spatial light modulator (SLM) with a resolution of 1920 ×1080 pixels and a pixel pitch of 6.4μm (Thorlabs Exulus HD-1/M), and the pattern displayed at the SLM is imaged at the RGG with the help of lenses L1 and L2. The size of the illumination beam at the SLM is fixed at around 5 mm. On the other hand, an off-axis reference point source is generated by introducing a tilt in the incoming beam and focusing the tilted beam at an off-axis position on the RGG plate. A red dot at the RGG represents a reference point.

A sequence of dynamically fluctuating intensity patterns composed of the object and an off-axis reference illumination is captured by a high-speed complementary metal-oxide semiconductor (CMOS) camera, which has a resolution of 1024 × 1024 pixels up to 20,000 frames per second, a dynamic range of 12 bits, and a pixel pitch of 20μm [Photron Fastcam SA-Z]. We adjusted the rotation speed of the RGG to 0.033 rps and provided dynamically fluctuating intensity patterns on the high-speed CMOS camera with an exposure time of 250μs. The speed of the Photron Fastcam SA-Z CMOS camera is fast enough to capture the dynamically fluctuating intensity patterns as compared to the conventional camera. The CMOS is placed at a distance of 400mm from the RGG plate, and a lensless intensity correlation hologram is recorded, as explained in Eq. (3.9).

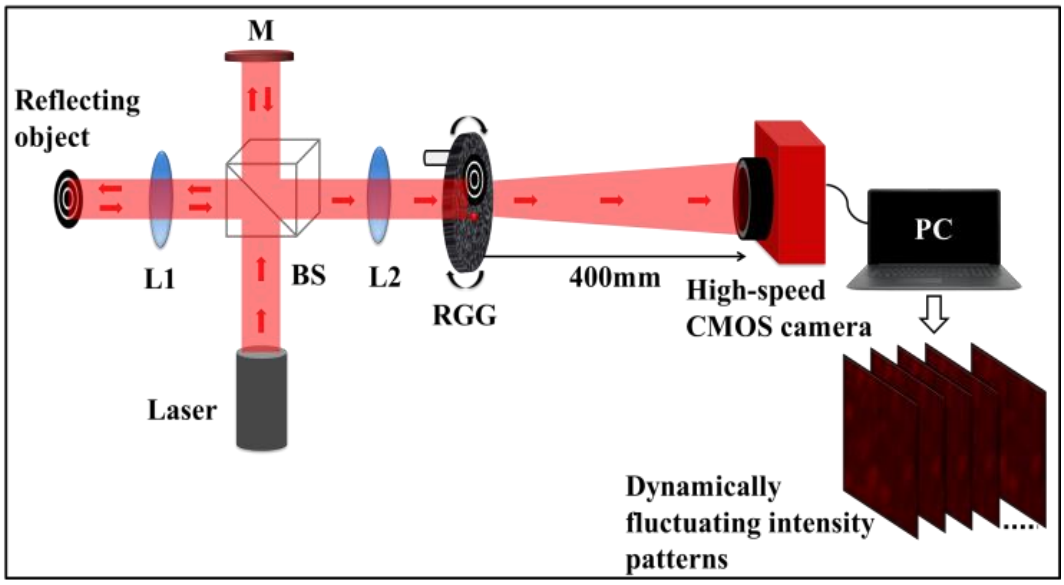

Fig. 3.3 Schematic of the optical set-up. BS: beam splitter; L1, L2: lenses; M: mirror; RGG: rotating ground glass; CMOS: complementary metal-oxide semiconductor, PC: personal computer.

Using Eq. (3.2), (3.7), an instantaneous complex field captured at the camera plane is represented as

$$U_s(\boldsymbol{r},t)=\frac{e^{ikz}}{i\lambda z}\left[\int U(\boldsymbol{\rho},t)\exp\left(\frac{ik}{2z}(\boldsymbol{r}-\boldsymbol{\rho})^2\right)d^2\boldsymbol{\rho}+\int U_R(\boldsymbol{\rho},t)\exp\left(\frac{ik}{2z}(\boldsymbol{r}-\boldsymbol{\rho})^2\right)d^2\boldsymbol{\rho}\right], \qquad (3.11)$$

Here, the constant phase term $\frac{e^{ikz}}{i\lambda z}$ is ignored from further consideration as we are interested in observations at a fixed z value.

Hence, the complex coherence function at the observation plane is expressed as

$$W_s(\boldsymbol{r_1},\boldsymbol{r_2})=\left\langle U_s^*(\boldsymbol{r_1})U_s(\boldsymbol{r_2})\right\rangle=\left\langle U^*(\boldsymbol{r_1})U(\boldsymbol{r_2})\right\rangle+\left\langle U_R^*(\boldsymbol{r_1})U(\boldsymbol{r_2})\right\rangle \qquad (3.12)$$

where, $\left\langle U^*(\boldsymbol{r_1})U_R(\boldsymbol{r_2})\right\rangle\approx 0$, due to considering statistically independent dynamically fluctuating fields emerging from the RGG.

The dynamically fluctuating intensity patterns are considered to obey Gaussian statistics [4]. Assuming stationarity and ergodicity at the camera plane, we replace the ensemble average with the time average of the dynamically fluctuating field emerging from RGG**.** Hence, $\left\langle \exp\left[i\varphi(\boldsymbol{\rho},t)\right]\right\rangle_T = 0$, and $\left\langle \exp\left[i\varphi(\boldsymbol{\rho_1},t) - i\varphi_m(\boldsymbol{\rho_2},t)\right]\right\rangle_T = \delta(\boldsymbol{\rho_1}-\boldsymbol{\rho_2})$, where $\langle\ \rangle_T$ denotes the temporal average. Considering $\boldsymbol{r_1} = \boldsymbol{r}, \boldsymbol{r_2} = \boldsymbol{r}+\Delta\boldsymbol{r}$ and making use of the relation, $\int \exp\left(-i\frac{2\pi}{\lambda f}[\boldsymbol{r}.(\boldsymbol{\rho_2}-\boldsymbol{\rho}_1)]\right)d^2\boldsymbol{r} \propto \delta(\boldsymbol{\rho_2}-\boldsymbol{\rho}_1)$, Eq. (3.12) transforms to

$$W_s(\Delta\boldsymbol{r}) = \int I_s(\boldsymbol{\rho}) \exp\left(-i\frac{2\pi}{\lambda f}\Delta\boldsymbol{r}.\boldsymbol{\rho}\right)d^2\boldsymbol{\rho}, \tag{3.13}$$

where, $\boldsymbol{\rho_1} = \boldsymbol{\rho}_2 = \boldsymbol{\rho}$, and $I_s(\boldsymbol{\rho}) = U_s^*(\boldsymbol{\rho})U_s(\boldsymbol{\rho}) = I(\boldsymbol{\rho}) + I_R(\boldsymbol{\rho})$ represents the composition of two independent objects and references at the RGG plane.

Thus, the complex coherence function of the desired object and a reference are represented as

$$W(\Delta\boldsymbol{r}) = \int I(\boldsymbol{\rho}) \exp\left(-i\frac{2\pi}{\lambda f}\Delta\boldsymbol{r}.\boldsymbol{\rho}\right)d^2\boldsymbol{\rho}, \tag{3.14}$$

$$W_R(\Delta\boldsymbol{r}) = \int I_R(\boldsymbol{\rho}) \exp\left(-i\frac{2\pi}{\lambda f}\Delta\boldsymbol{r}.\boldsymbol{\rho}\right)d^2\boldsymbol{\rho}, \tag{3.15}$$

Here, we have considered an off-axis point source as a reference, which is expressed as $I_R(\boldsymbol{\rho}) = circ\left(\frac{\boldsymbol{\rho}-\boldsymbol{\rho_0}}{a_0}\right)$, where $\boldsymbol{\rho_0}$ is the off-axis location of the reference point at the RGG plane, while a_0 represents the aperture size at the RGG plane. The aperture size a_0 is very small to generate a uniform reference coherence $W_R(\Delta\boldsymbol{r})$ to cover the support of $W(\Delta\boldsymbol{r})$ as desired in Eq. (3.9).

Eq. (3.14) states that the complex coherence function at the camera plane is the Fourier transform of the object at the RGG and is known as the van-Cittert Zernike (vCZ) theorem [168]. Thus, the object distribution $I(\boldsymbol{\rho})$ is retrieved from the complex coherence function.

3.3.2 Experimental results

We present images of different objects hidden behind a dynamic scattering medium to validate the proposed technique. Here, we consider three objects, namely the "ring-shaped object," "Hollow Gaussian beam (HGB)" of amplitude where ω is the beam waist size, and an off-axis computer-generated Fourier hologram (CGH). This CGH encodes a pure phase object with a helical phase structure, i.e., a vortex beam with topological charge (TC) $l=1$. The TC represents phase variation around the center in the order of 2π. To make a CGH, a vortex is digitally Fourier transformed and this field is superimposed with a carrier reference beam. This interference pattern is used to provide transparency for the third object. Experimentally recorded intensity patterns of the "ring-shaped object", captured with a high-speed detector, are shown in Fig. 3.4(a). The intensity cross-covariance of the temporally fluctuating intensity patterns is implemented as follows. Experimentally recorded intensity is represented as $I_s^k(\boldsymbol{r})$, where $\boldsymbol{r}=(x,y)$ is the pixel spatial coordinate which takes values up to 1000 × 1000 pixels. Correlating the two-point intensity fluctuations $\Delta I_s^k(\boldsymbol{r_1})\Delta I_s^k(\boldsymbol{r_2})$ for different realizations of the random fields and this process is represented as, $\sum_{k=1}^{10000}\left[\Delta I_s^k(\boldsymbol{r_1})\Delta I_s^k(\boldsymbol{r_2})\right]$, where, k represents each realization of the random intensity patterns which ranges from 1 to 10,000 in our experiment.

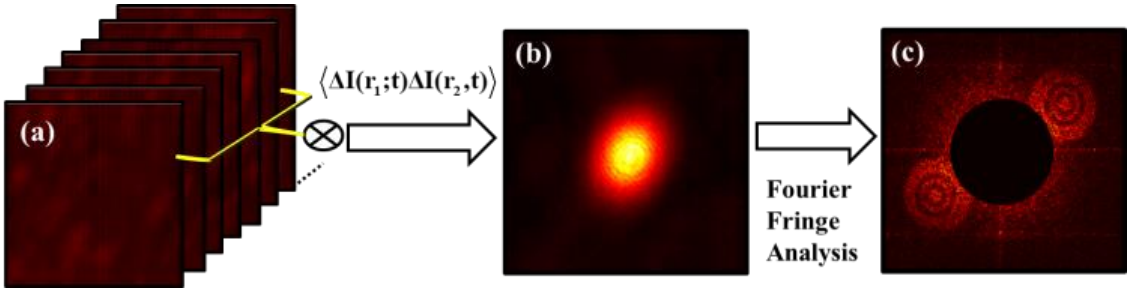

Fig. 3.4 (a) Representation of cross-covariance process for the dynamically scattered intensity patterns. (b) Cross-covariance of intensity patterns. (c) Fourier spectrum of the cross-covariance.

The cross-covariance of the experimentally detected 10000 intensity patterns is obtained by applying temporal averaging, as shown in Fig. 3.4(b). The fringes of the cross-covariance of the intensity correlation can be observed in the bright area at the center. These fringes in Fig. 3.4(b) represent the intensity correlation hologram as explained by Eq. (3.9). Making use of the Fourier fringe analysis, the complex coherence function is recovered even with intensity correlation as represented in Fig. 3.4(c).

Fig. 3.5(a) shows the target displayed on the SLM, and 3.5(b) shows the Fourier spectra of the cross-covariance for this "ring-shaped object". Similarly, Figs. 3.5(c)-(d) show the target and Fourier spectra of the cross-covariance for the object "HGB". The Fourier transform of the cross-covariance generates two off-axis spectra and a DC term. The separation distance of conjugate images in Figs. 3.5(b) and 3.5(d) are determined by the linear phase generated by a reference point source at the RGG. Two copies of the object, i.e., the object and its conjugate, are obtained due to an off-axis holographic relation in the intensity correlation hologram, as explained in Eq. (3.9).

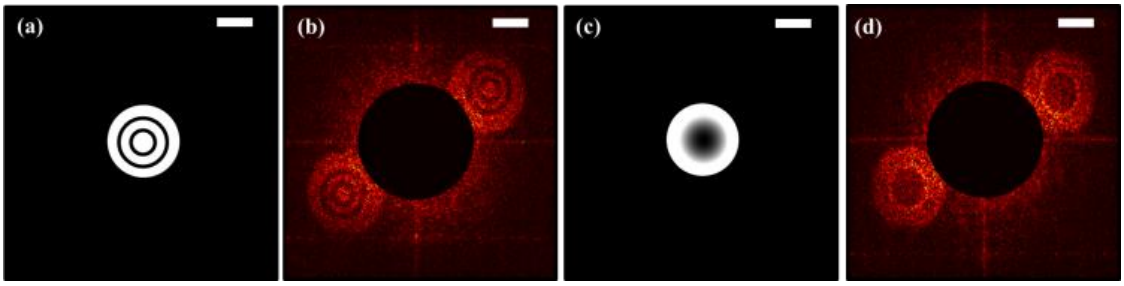

Fig. 3.5 Experimental Results: (a), (c) show the target, and (b), (d) show the corresponding reconstructed amplitude distribution of the 'ring shaped object' and 'HGB', respectively—scale bar: 2.5 mm.

We have also examined imaging of a complex-valued object behind the dynamic scattering medium, and results are shown in Fig. 3.6. To preserve the complex-valued object information and recover it using the vCZ with the intensity correlation, we consider a CGH in the experiment, which is placed behind the dynamic diffuser using SLM. As explained previously, dynamically scattered light is detected, and cross-covariance is obtained.

The Fourier spectra of the cross-covariance of the intensity patterns are shown in Figs. 3.6(a) for a CGH. The appearance of the fork structure in the Fourier spectra confirms the encoding of the vortex with TC *l=1* in the CGH. The complex coherence function of the vortex with TC *l=1* is retrieved through inverse Fourier transforming one of the centrally shifted off-axis components from Fig. 3.6(a), and the reconstructed amplitude and phase distributions are represented in Figs. 3.6(b)–3.6(c), respectively.

The proposed technique's imaging quality depends on the cap of the delta correlation characteristics of illuminating random phases of the intensity patterns, the number of realizations of intensity patterns, and the size of the optical elements.

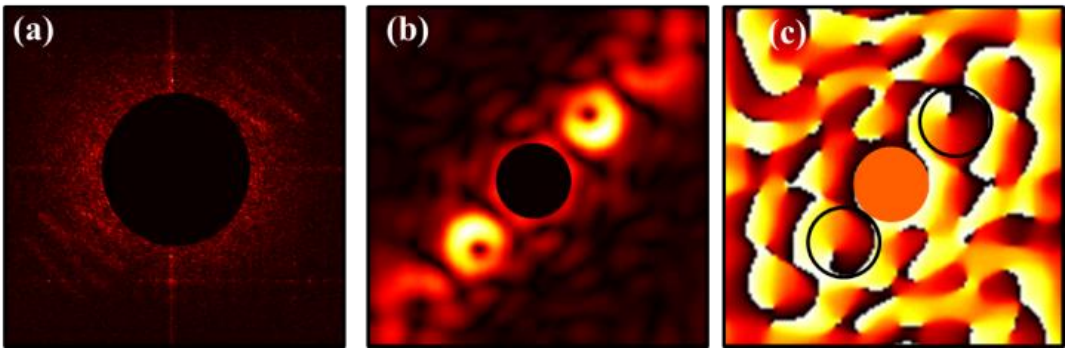

Fig. 3.6 Experimental Results: (a) Fourier spectra of the cross-covariance distributions of the vortex object with TC *l=1*. (fork pattern). Figs. (b), (c) indicates the vortex object's reconstructed amplitude and phase distribution from the inverse Fourier transforms of one of the centrally shifted fork patterns.

3.4 Looking through fog with a high-speed camera

Fog significantly impairs visibility, posing serious challenges for transportation, aviation, remote sensing, surveillance, security, and astronomy. Achieving clear vision through dense fog ensures safety in various applications. Examples include enabling self-driving cars to navigate adverse weather conditions, enhancing drivers' situational awareness for detecting hidden objects and reading road signs, providing clear flight paths for drones, airplanes, and helicopters during low-altitude operations, and allowing trains to maintain optimal speeds in foggy conditions [338]. Consequently, developing advanced technologies to overcome visibility challenges in natural scattering environments like dense fog and turbid water has become a pressing need.

The primary challenge in imaging through dynamic scattering media lies in the significant attenuation of light caused by scattering and absorption. To address this issue, several innovative techniques have been proposed in recent years to enable imaging through extended dynamic scattering media [333,334,339,340]. This work presents an alternative approach for imaging through foggy conditions, which is mimicked in the laboratory. Our

technique leverages the HBT approach with holography, as depicted schematically in Fig. 3.7. The experimental setup and results are detailed in the subsequent sections.

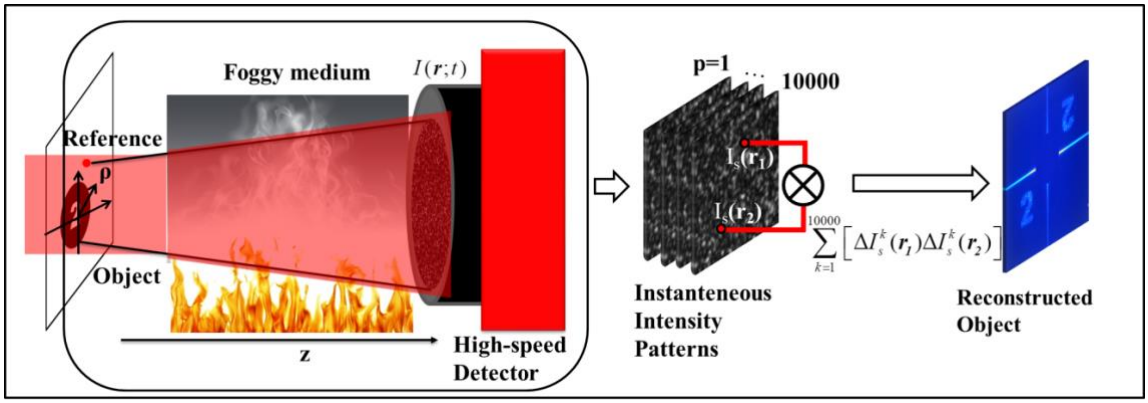

Fig. 3.7 Conceptual representation of our technique.

3.4.1 Experimental setup and results

The experimental setup for imaging through a foggy medium is depicted in Fig. 3.8. Here, we used a He-Ne laser beam at 632nm to illuminate a rotating ground glass (RGG) to generate an incoherent source. The scattered light from the RGG plate is treated as incoherent because the incident beam spot size on the RGG plate is significantly larger than the inhomogeneity scale of the plate. These dynamically fluctuating intensity patterns produced by the RGG are directed through a medium exhibiting severe refractive index fluctuation to experimentally mimic foggy conditions. To create this foggy environment, a professional heat gun (Steinel HG 2320 E) delivers hot air within a temperature range of 120–1200°F. This introduces refractive index fluctuations in the light propagation channel, causing the intensity patterns to attenuate rapidly. A high-speed camera is used to capture these fluctuating intensity patterns.

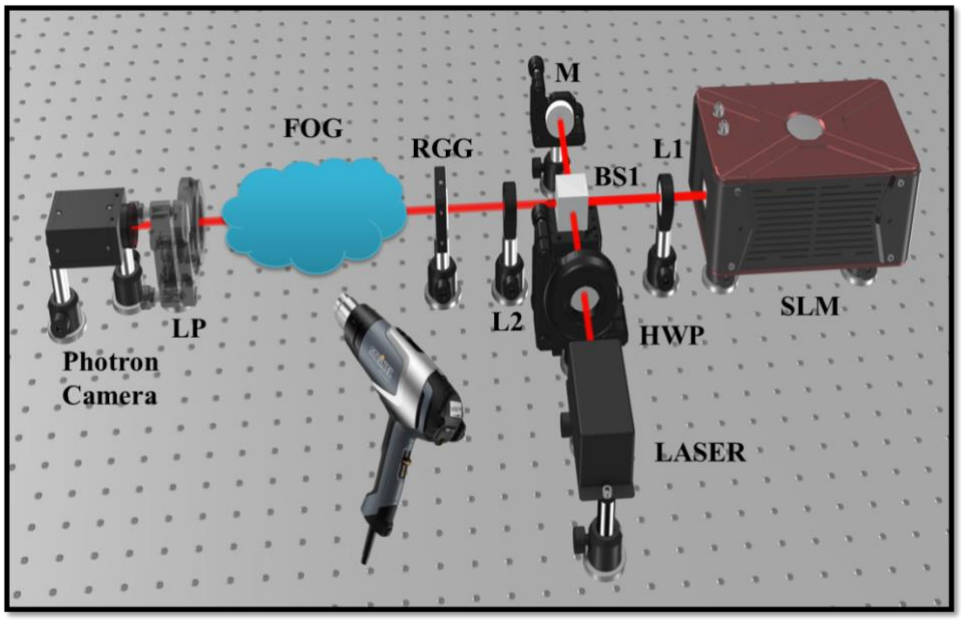

Fig. 3.8 Schematic of the optical set-up. BS1: beam splitter; L1, L2: lenses; SLM: spatial light modulator; M: mirror; RGG: rotating ground glass; LP: linear polarizer.

The technique's feasibility is demonstrated with objects in both reflection and transmission geometries. A spatial light modulator (SLM) (Thorlabs Exulus HD-1/M) with a resolution of 1920 × 1080 pixels and a pixel pitch of 6.4 μm is utilized for the reflection geometry. The SLM is illuminated with a beam of approximately 5 mm and imaged onto the RGG plate using a 4f imaging system composed of two lenses, L1 and L2. A "cross"-shaped target is displayed on the SLM for this experiment, as shown in Fig. 3.9(a). The SLM is turned off for the transmission geometry, and a transparency containing the object information is placed between the RGG plate and the hot-air flow. A "letter 2" target, printed on the transparency, is shown in Fig. 3.9(b). An off-axis reference point source is generated on the RGG plate using a mirror (M) and a lens (L2), and a sequence of dynamically fluctuating intensity patterns composed of the object and an off-axis reference illumination is captured by a high-speed complementary metal-oxide semiconductor (CMOS) camera. This CMOS camera has a resolution of 1024 × 1024 pixels up to 20,000 frames per second, a dynamic range of 12 bits, and a pixel pitch of

20μm [Photron Fastcam SA-Z]. Positioned 400 mm from the RGG plate, the CMOS records dynamically fluctuating intensity patterns, and 10,000 frames are captured for each object to record the intensity correlation hologram as described in Eq. (3.9).

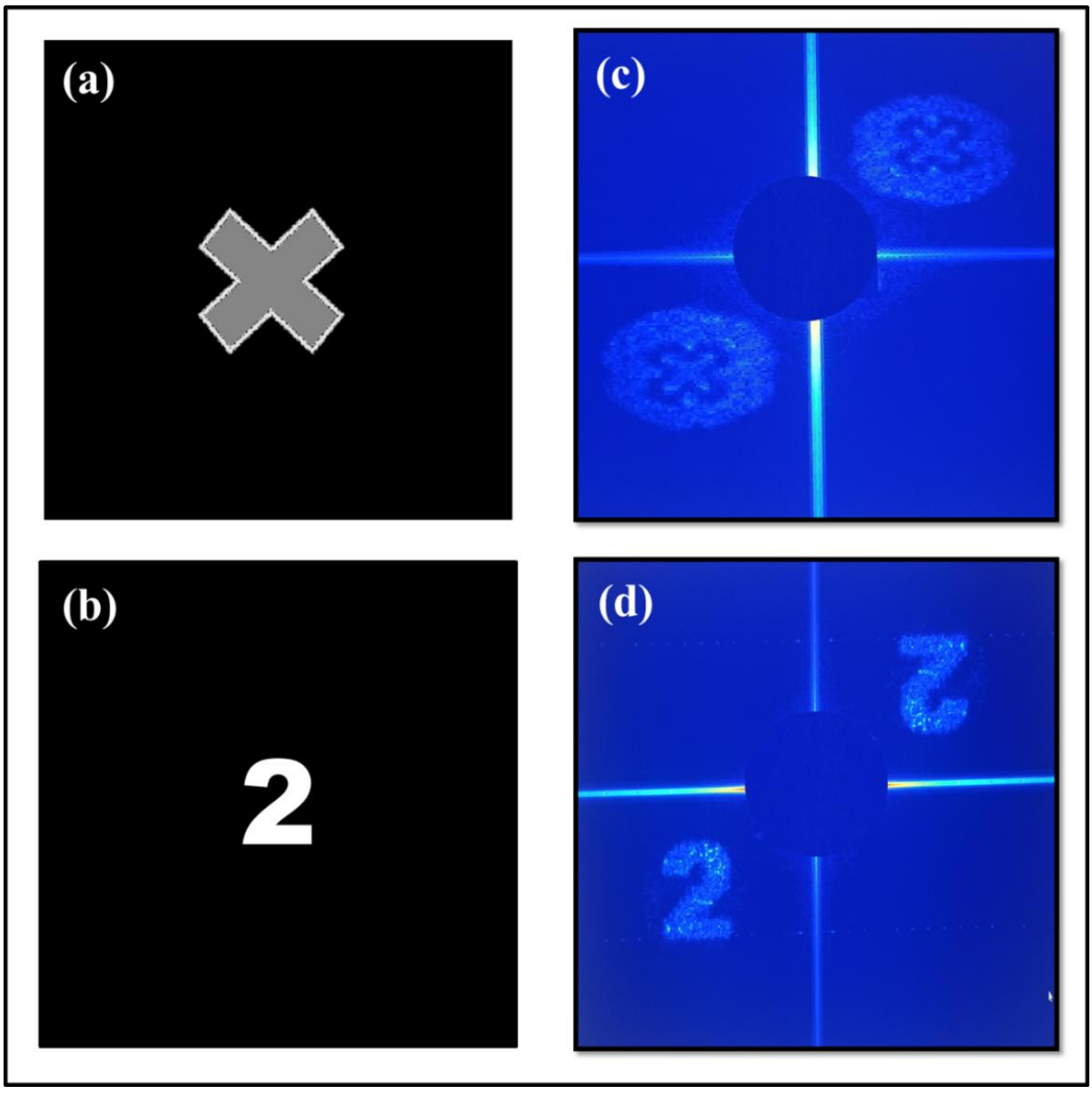

Fig. 3.9 Experimental Results: (a), (b) show the target, and (c), (d) show the corresponding reconstructed amplitude distribution of the 'cross' and 'letter 2', respectively.

Fourier fringe analysis is then applied to the intensity correlation fringes to reconstruct the object images. Fig. 3.9(c) shows the reconstructed image of the "cross" displayed on the SLM, while Fig. 3.9(d) shows the reconstructed image of the "letter 2" from the transparency. Due to the off-axis holographic arrangement, two copies of the object (the object itself and its conjugate) are retrieved in the intensity correlation hologram, as explained in Eq. (3.9).

3.5 Conclusion

In this chapter, we have presented two novel experimental techniques for imaging through different dynamic scattering media. The theoretical framework of the proposed method is established within the realm of intensity correlations of dynamically fluctuating intensity patterns. Intensity fluctuating patterns from dynamic diffusers and foggy mediums are captured with a high-speed camera, and the applicability of the proposed technique is verified by reconstructing different incoherent objects and holograms hidden behind the dynamic scattering media. These techniques are expected to find applications in imaging in a turbulent environment and coherence analysis.